Journal of Molecular Structure 1325 (2025) 141034

Contents lists available at ScienceDirect

Journal of Molecular Structure

journal homepage: www.elsevier.com/locate/molstr

Synthesis, crystal structures, Hirshfeld surface analysis, antioxidant activity and molecular docking studies of thiomethylbenzimidazole ligand and its mononuclear Zn(II) complex

Feriel Aouatef Sahki [a,b], Mehdi Bouchouit [a], Ouided Benslama [c], Rafika Bouchene [d,e], Sofiane Bouacida [a,e], Abdelmalek Bouraiou [a,*]

[a] Unité de Recherche de Chimie de l'Environnement et Moléculaire Structurale, CHEMS, Université des frères Mentouri, Constantine 1, 25000, Algérie
[b] Département de Chimie, Faculté des Sciences, Université Mohamed Boudief M'sila, 28000, Algérie
[c] Laboratoire Substances Naturelles, Biomolécules et Applications Biotechnologiques, Département des Sciences de la Nature et de la Vie, Faculté des Sciences Exactes et Sciences de la Nature et de la Vie, Université d'Oum El Bouaghi, Oum El Bouaghi 04000, Algérie
[d] Laboratoire des Sciences Analytiques, Matériaux et Environnement, Université d'Oum El Bouaghi, Oum El Bouaghi 04000, Algérie
[e] Département Sciences de la Matière, Faculté des Sciences Exactes et Sciences de la Nature et de la Vie, Université d'Oum El Bouaghi, Oum El Bouaghi 04000, Algérie

ARTICLE INFO

Keywords:
Benzimidazole
Zinc complex
Single crystal
Hirshfeld surfaces
Antioxidant activity
Docking molecular

ABSTRACT

The title compounds, 2-(((1-methyl-1H-imidazol-2 yl)methyl)sulfanyl)methyl)-1H-benzo[d]imidazole and its Zn^{II} complex were synthesized. The structure of the resulting products confirmed by spectroscopic techniques including FTIR, ^{1}HNMR , ^{13}CNMR and single crystal X-ray diffraction. The single crystal X-ray analyses reveal that the centrosymmetric Zn^{II} cation $Zn(MIMTMB)_2Cl_2$ complex is tetrahedrally coordinated by two N chelating azole ligand and by two chlorine atoms in a distorted tetrahedral geometry. The cohesion of the structure and stability are ensured by intermolecular O–H···O, N–H···O and C–H···O hydrogen bonds. The intermolecular interactions in complex and ligand are further inspected by Hirshfeld surface analysis. The docking results indicate that ligand MIMTMB exhibits a promising antioxidant activity, supported by its strong binding affinity to cytochrome c peroxidase (CCP) and significant inhibition of DPPH radicals in vitro. Conversely, the zinc complex, $Zn(MIMTMB)Cl_2$, exhibits weaker antioxidant activity.

1. Introduction

In recent years, the synthesis and characterization of transition metal complexes have generated considerable interest. The preparation of a new ligand may have been the most important step in the development of metal complexes that exhibit unique properties and new reactivity. Given that the electron donor and acceptor properties of the ligand, the structural functional groups, the position of the ligand in the coordination sphere, and the reactivity of the coordination compounds can be the determining factors for different studies [1–4]. Their interest stems from their versatility and broad complexation capabilities.

Transition metal complexes based on heterocyclic ligands, particularly those containing nitrogen and sulfur, have various applications in different fields, including biology. Sulfur and nitrogen donor ligands make them important and essential materials in the search for compounds with useful activity [5–12].

In other hand, the role of antioxidants in mitigating oxidative stress has garnered significant attention. Antioxidants are molecules that neutralize reactive oxygen species (ROS), thereby preventing oxidative damage and maintaining cellular integrity [13]. Natural and synthetic antioxidants have been extensively studied for their potential therapeutic benefits in combating oxidative stress-related diseases.

One enzyme that plays a pivotal role in cellular antioxidant defense mechanisms is cytochrome c peroxidase (CCP) [14]. CCP is a heme-containing enzyme primarily found in the mitochondria, where it catalyzes the reduction of hydrogen peroxide (H_2O_2) to water, thereby preventing the accumulation of (ROS) and protecting cells from oxidative damage [15]. The structural and functional characteristics of CCP make it an attractive target for studying the mechanisms of antioxidant action and developing novel antioxidant agents.

For 1-methylimidazole-containing ligands, our groups have presented several studies on their applications in constructing several

* Corresponding author.
E-mail address: bouraiou.abdelmalek@umc.edu.dz (A. Bouraiou).

https://doi.org/10.1016/j.molstruc.2024.141034
Received 21 November 2024; Received in revised form 3 December 2024; Accepted 5 December 2024
Available online 6 December 2024

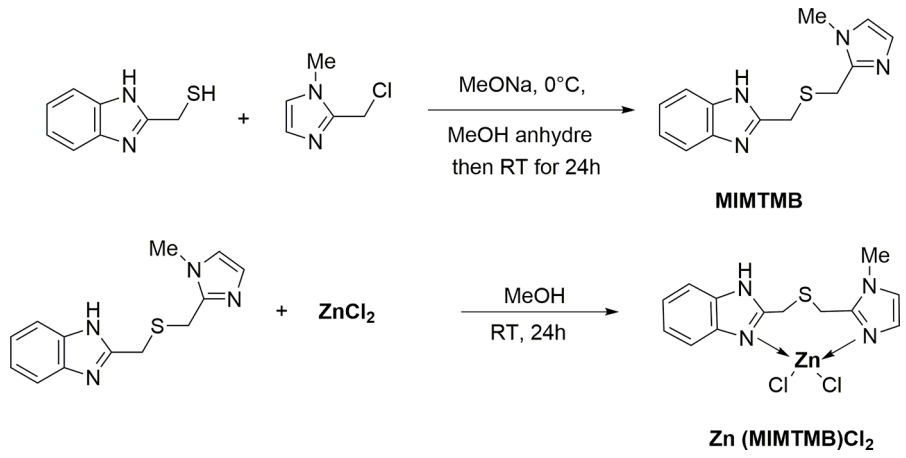

Schema 1. Synthesis of ligand MIMTMB and its complex Zn(MIMTMB)Cl_2.

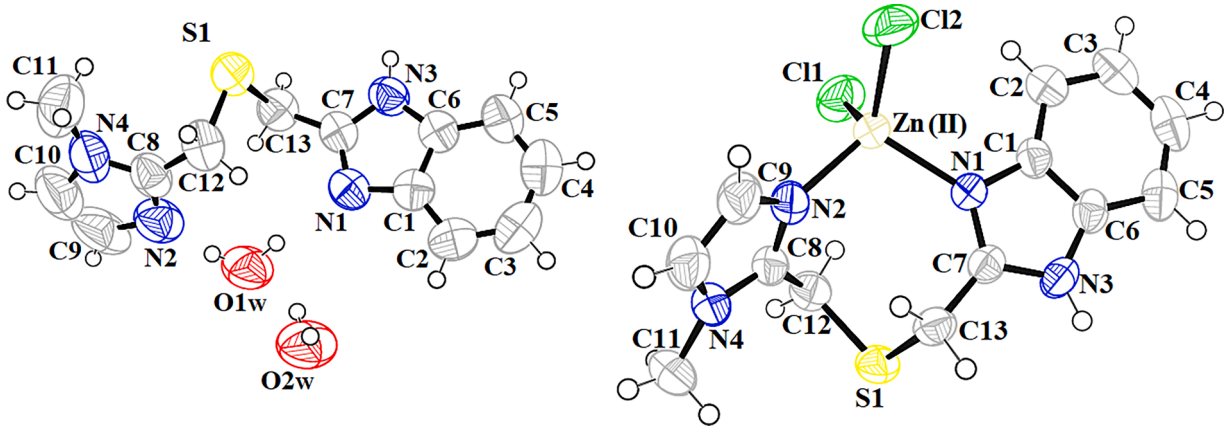

Fig. 1. Oak ridge thermal ellipsoid plots (ORTEP) of the molecular structure of MIMTMB and complex Zn(MIMTMB)Cl_2.

Table 1
Crystallographic data and refinement parameters for the MIMTB ligand and complex Zn(MIMTMB)Cl_2.

	MIMTMB	Zn(MIMTMB)Cl_2
Chemical formula	$C_{13}H_{14}N_4S$, 2(H_2O)	$C_{13}H_{14}Cl_2ZnN_4S$
M	294.37	394.61
Crystal habit, color	Prism, Yalow	Prism, Yalow
Crystal system	Orthorhombic	Monoclinic
Space group	P $2_12_12_1$	P $2_1/c$
a (Å)	4.5979 (2)	7.6464(3)
b (Å)	17.5751(10)	16.0038(6)
c (Å)	18.4318(9)	13.5503(5)
β (°)	90	111.114(2)
V (Å^3)	V = 1489.45(13)	1546.85(10)
Z	4	4
Density (calculer, g cm^{-3})	1.313	1.694
Absorption coefficient (mm^{-1})	0.225	2.065
F(000)	624	800
Crystal size (mm)	0.15×0.08× 0.05	0.08×0.08×0.07
θ range for data collection (°)	3.2- 20.93	3.01–31.06
Reflections collected	10,105	19,341
Independent reflections	4393	5035
R_{int}	0.0520	0.0204
Reflections with $I \geq 2\sigma(I)$	2331	4037
Nombre de parametrers	198	191
Goodness-of-fit on F^2	0.92	1.052
Final R indices [$I \geq 2\sigma(I)$]	0.0465	0.0271
R indices [all data]	R_1=0.1138,	R_1= 0.0386, wR_2=
Largest difference peak and hole (Å^{-3})	wR_2=0.0782 0.166, −0.165	0.0682, 0.407, −0.286

Table 2
Selected interatomic distances (Å) and bond angles (°) for complex Zn (MIMTMB)Cl_2 and MIMTMB.

	MIMTMB	Zn(MIMTMB)Cl_2
Bond lengths (Å)		
C7–N1	1.324 (2)	1.3289 (17)
C7–N3	1.350 (2)	1.3514 (18)
C8–N2	1.320 (3)	1.3277 (19)
C8–N4	1.354 (3)	1.3458 (17)
C7–C13	1.483 (3)	1.481 (2)
C8–C12	1.477 (3)	1.4798 (19)
C1–N1	1.402(2)	1.3968(17)
C9–N2	1.376(3)	1.379(2)
Zn1–N1	–	2.0416(11)
Zn1–Cl1	–	2.2561(5)
Zn1–N2	–	2.0173(12)
Zn1–Cl2	–	2.2375(4)
Bond angles (°)		
C7–N3–C6	107.48(17)	108.53 (11)
N3–C7–C13	122.80(18)	122.01 (12)
C7–C13–S1	112.72 (13)	115.11 (10)
C8–N4–C10	106.6 (2)	107.70 (13)
N2–C8–N4	111.37 (19)	110.33 (13)
C8–C12–S1	113.17 (15)	112.09 (10)
C12–S1–C13	100.29(10)	101.70(7)
N1–Zn1–Cl1	–	107.39(4)
N1–Zn1–Cl2	–	109.43(3)
N2–Zn1–Cl2	–	110.63(4)
N1–Zn1–N2	–	106.79(5)
Cl1–Zn1–Cl2	–	113.182(18)
N2–Zn1–Cl1	–	109.16(4)

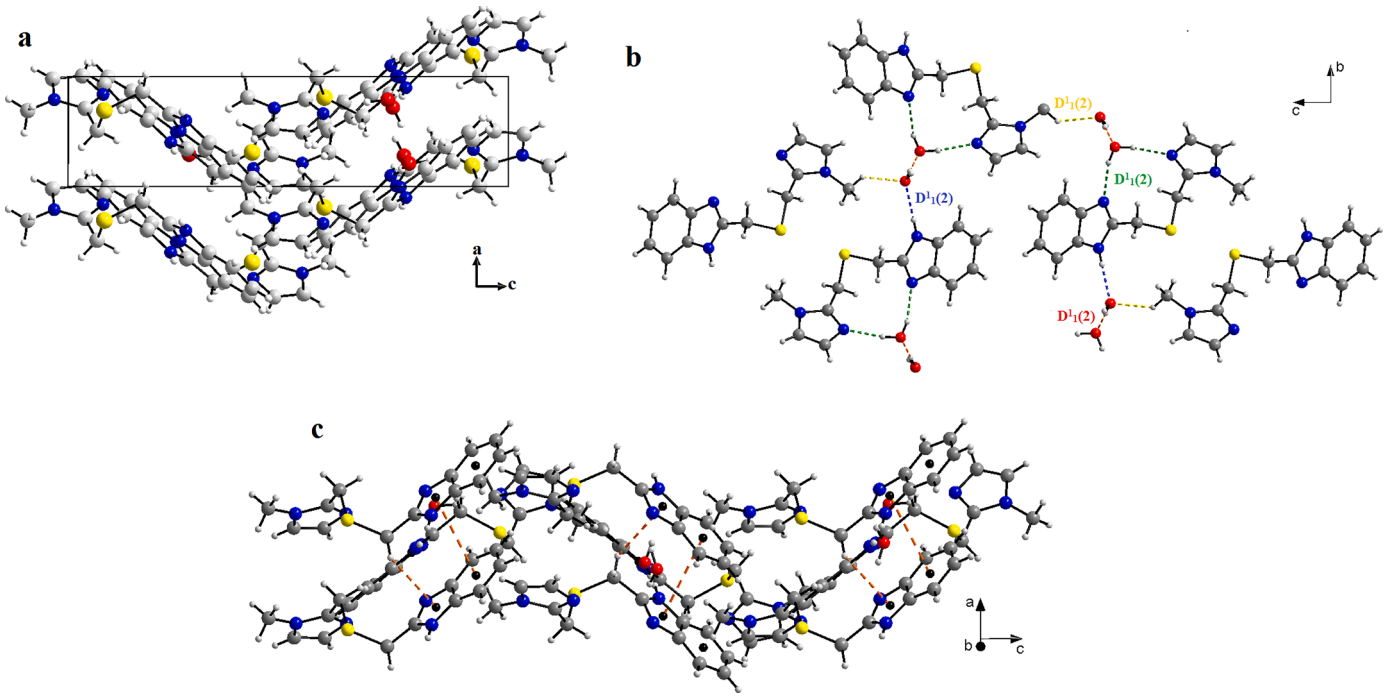

Fig. 2. (a) A set of diagrams of MIMTMB viewed along the b-axis showing zigzag layers parallel to the (101) plane.(b) Projection of the MIMTMB ligand onto the (b, c) plane, representing hydrogen bonds of the type O-H...O ($D^1_1(2)$, in red), N-H...O ($D^1_1(2)$, in blue), O-H...N ($D^1_1(2)$, in green), and C-H...O ($D^1_1(2)$, in yellow); (c) C-H...π and π-π interactions in MIMTMB.

Table 3
Distances (Å) and angles (°) for hydrogen bonds in crystals of complex MIMTMB and Zn(MIMTMB)Cl_2.

D–H…A	*d*(H…A)	*d*(D–A)	D–H–A	Symmetry
MIMTMB				
O2w-H3w… O1w	1.874(2)	2.743 (3)	173.191(3)	1-x,−1/2 + *y*, 1/2-z
O2w-H4w… O1w	1.999(3)	2.819 (3)	162.726(2)	1/2-x,1-y, 1/2 + *z*
N3-H3…O2w	1.941(2)	2.793 (3)	170.348(2)	3/2-x, 1-y, 1/2 + *z*
O1w-H1w…N2	1.934(2)	2.784 (3)	167.052(2)	1/2 + *x*,3/2-y, 1-z
O1w-H2w…N1	1.983(3)	2.812 (3)	164.305 (20)	1/2 + *x*,3/2-y, 1-z
Zn(MIMTMB) Cl_2				
N3-H3…Cl2	2.6177(5)	3.257 (2)	132.17(8)	1-x, 1/2 + *y*, 3/2-z
C13-H13B…Cl1	2.7866(4)	3.658 (2)	149.85(9)	-x, −1/2 + *y*, 1/2-z
C13-H13A…N2	2.6164 (11)	3.288 (2)	126.67(9)	1 + *x*, 3/2-y, 1/2 + *z*

Table 4
Distances (Å) and angles (°) for C—H…π interactions in complex Zn(MIMTMB) Cl_2 and MIMTMB.

C–H…Cg	d (C–H)	d (H… Cg)	d (C–Cg)	C–H–Cg	Symetry
MIMTMB					
C(13)–H (13A)….Cg (1)	0.97	2.92	3.539 (5)	123	2-x,-y, 1-z
Cg(1) : (N(1)–C(1)–C(6)–C(4)–N(3)–C(7))					
Zn(MIMTMB)Cl_2					
C(12)–H (12B)…Cg (3)	0.97	2.99	3.463 (6)	111	2-x,-y, 1-z
Cg(3) : (C(1)–C(2)–C(3)–C(4)–C(5)–C(6))					

coordination complexes [16–19]. For extending our project, the aim of the present work is the synthesis of -(((1-methyl-1H-imidazol-2-yl) methyl)sulfanyl)methyl)−1H-benzo[d]imidazole (MIMTMB) and its Zinc metal complex and studied their crystal structures based on X-ray experiments and conventional spectroscopic methods. The intermolecular interactions in both complex and ligand are further inspected by Hirshfeld surface analysis. Through molecular docking studies and in vitro assays, we aim to elucidate the binding mechanisms and evaluate the antioxidant efficacy of these compounds. Additionally, we aim to assess their pharmacokinetic properties and discuss their potential as therapeutic agents for oxidative stress-related disorders.

2. Experimental section

2.1. Materials and instrumentation

All chemicals reagents and solvents were of analytical grade and were used as received. The melting point was determined using an electrothermal IA9100 digital melting point apparatus. ^{1}H NMR and ^{13}C NMR spectra were recorded on a Bruker Avance 250 MHz and Bruker Avance III 400MHz. UV and FT-IR spectra were recorded on Optizen 1220 UV/VIS spectrophotometer and Thermo Scientific Nicolet iS50 FTIR spectrophotometer. Crystallographic data of the studied structures have been collected on a Bruker APEX three-circle diffractometer equipped with an Apex II CCD detector using Mo-Ka radiation (micro-focus sealed tube with a graphite monochromator). For data collection, crystals were treated with Paratone oil and then fixed on loops. The reported structure was solved by direct methods with SIR2004 [20] to locate all the non-H atoms, which were refined anisotropically with SHELXL97 [21] using full-matrix least-squares on the F2 procedure from within the WinGX [22] suite of software used to prepare material for publication. All absorption corrections were performed with the SADABS program [23]. All non-hydrogen atoms were refined anisotropically. Hydrogen atoms were placed in idealized geometrical positions and refined with Uisotied to the parent atom with the riding model. The studied compounds' cif-files can be found in the Cambridge

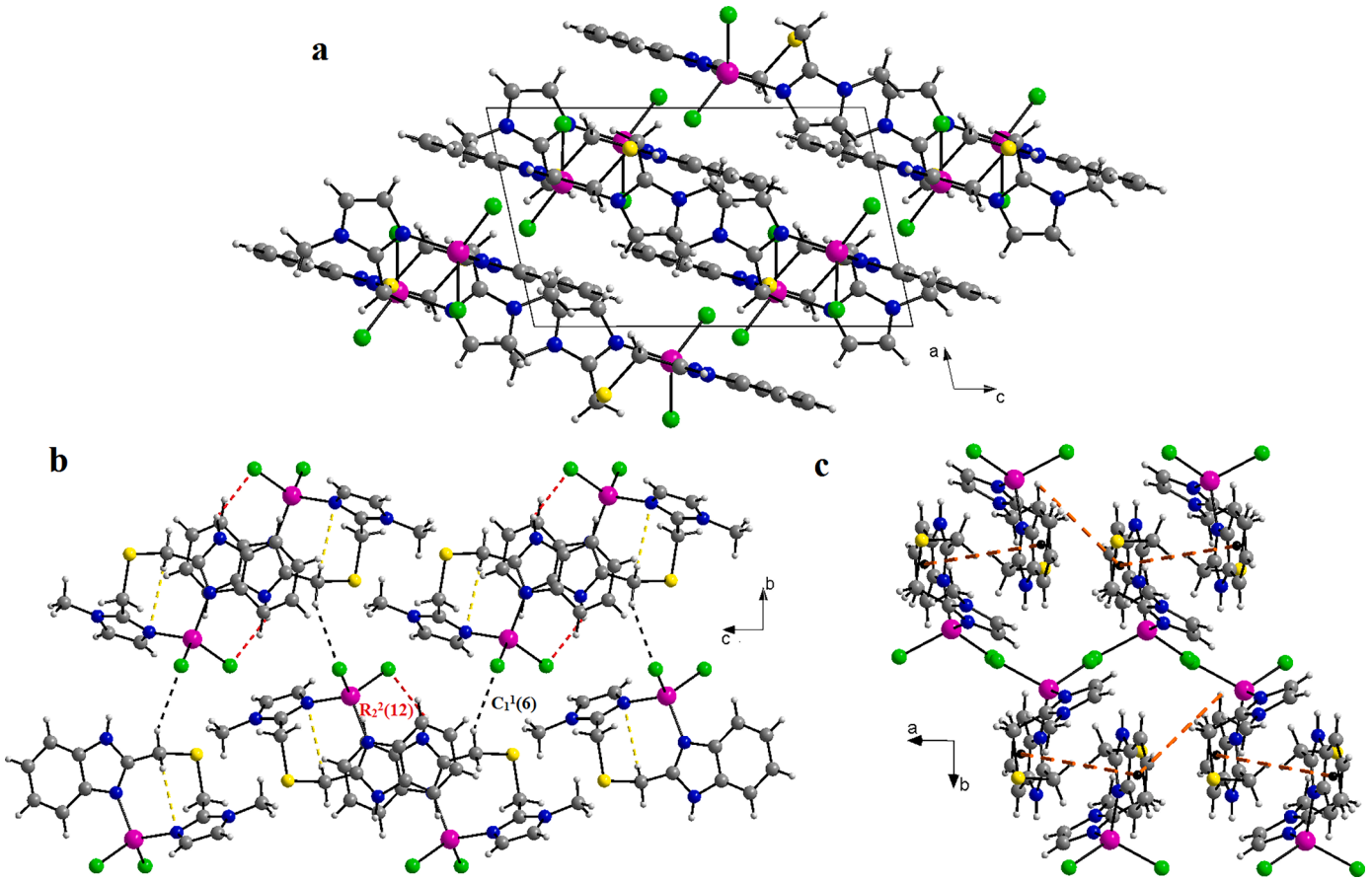

Fig. 3. (a) The projection of the structure onto the (a, c) plane of complex Zn(MIMTMB)Cl_2; (b) Representation of intermolecular hydrogen bonds of N-H…Cl type (in red), C-H…Cl type (in black), and intramolecular C-H…N type (in yellow); (c) C-H.…π and π-π interactions in complex Zn(MIMTMB)Cl_2.

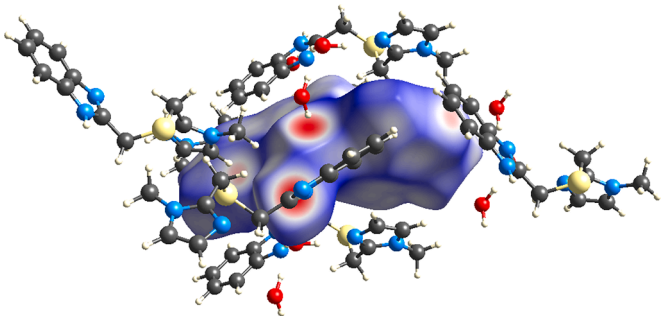

Fig. 4. Molecular environment around the Hirshfeld surface of the MIMTMB ligand.

Structural database under the numbers CCDC 1,525,120 and CCDC 1, 525,122. On request to the Director, CCDC, 12 Union Road, Cambridge CB2 1EZ, UK, fax: +44 (0)1223 336,033, or email: deposit@ccdc.cam.ac.uk, free copies of the available material can be obtained.

2.2. Preparation of MIMTMB ligand and complex B1

2.2.1. Synthesis of MIMTMB ligand

Sodium (0.575 g, 25 mmol) was added to anhydrous methanol (20 mL) at 0 °C. After 5 min, 1.66 g (1H-benzo[d]imidazol-2-yl)methanethiol (10 mmol) were added and the mixture was vigorously stirred for 10 min at 0 °C. 2-Chloromethylbenzimidazole (1.66 g, 10 mmol) was added at one portion and the mixture was left to stir for 24 h at room temperature. The mixture was added into cold ice-water and the yellow

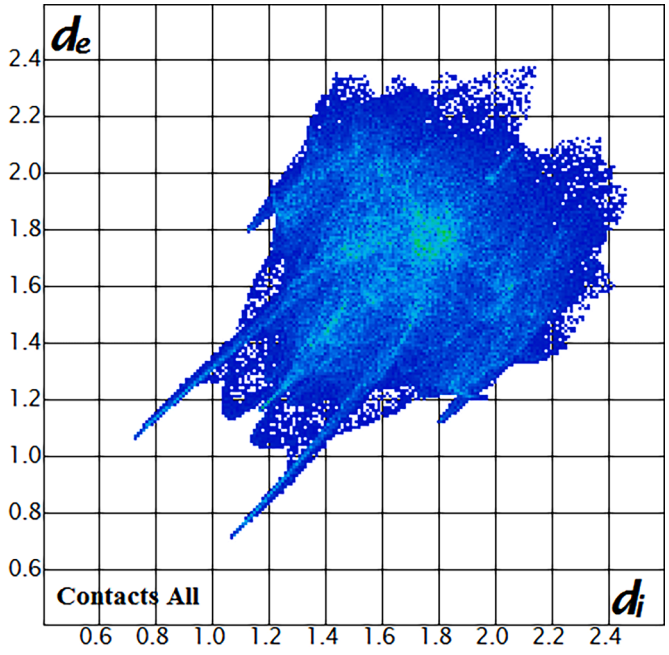

Fig. 5. 2D fingerprint plot of the Hirshfeld surface surrounding the MIMTMB ligand, illustrating the (d_i, d_e) pairs of all interatomic contacts.

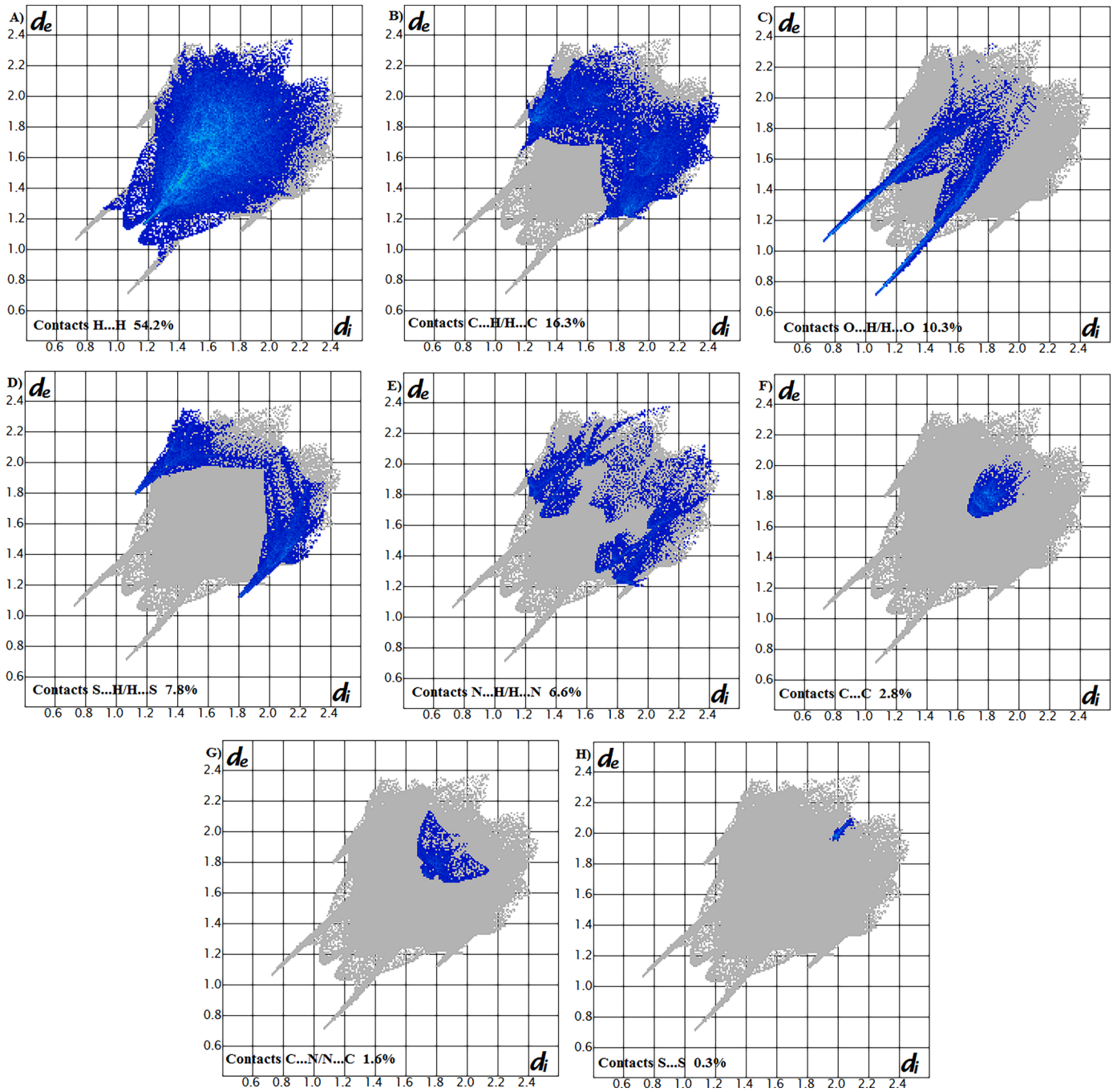

Fig. 6. Fingerprint plots with percentages of different contacts present in the MIMTMB ligand.

solid MIMTMB was formed, filtered, washed with methanol and then dried. Yield: 82 %; mp. 80–85 °C; IR (cm^{-1}): 1440, 1272, 1144, 1107, 1021, 744, 674; ^{1}H NMR ($CDCl_3$, 250.13 MHz) : 12.38 (s, 1H), 7.68–7.65 (m, 2H), 7.28–7.25 (m, 2H), 7.08 (s, 1H), 6.97 (s, 1H), 3.79 (s, 2H), 3.75 (s, 5H); ^{13}C NMR ($CDCl_3$, 62.9 MHz) : 151.62, 143.85, 138.75, 126.51, 122.38, 120.27, 115.41, 33.22, 26.98, 25.36 ; UV–Vis (DMF, λ (nm)) : 280.

2.2.2. *Synthesis of complex Zn(MIMTMB)Cl_2*

1 éq. of 2-(((1-methyl-1H-imidazol-2-yl)methyl)sulfanyl)methyl)–1H-benzo[d]imidazole (MIMTMB) (200 mg, 0.77 mmol) was dissolved in 10 mL de MeOH and 1 éq of $ZnCl_2$ (105.63 mg, 0.77 mmol) was added. The mixture was stirred for 24 h at room temperature and the obtained white solid was filtered, washed with small amount of cold methanol and then dried. Yield 71 %; m.p. 208–210 °C; IR (cm^{-1}): 1505, 1450, 1227, 1159, 1050, 967, 854, 738, 679; ^{1}H NMR (CD_3OD, 400.16 MHz) : 13.85 (s, 1H), 8.57–8.54 (m, 1H), 7.90–7.87 (m, 1H), 7.76 (s, 1H), 7.61–7.59 (m, 2H), 7.46 (s, 1H), 4.45 (s, 2H), 4.10 (s, 5H); ^{13}C NMR (CD_3OD, 100.13 MHz) : 152.79, 144.46, 140.09, 133.51, 125.39, 124.55, 123.95, 123.37, 119.07, 112.59, 33.35, 24.88, 23.80; Calcd. for $C_{13}H_{14}N_4Cl_2SZn$: C, 39.57; H, 3.58; N, 14.20 ; S, 8.12. Found: C, 39.99; H, 3.87; N, 13.67; S, 8.08; UV–Vis (DMF, λ_{max}/nm): 278, 284.

2.3. *In vitro antioxidant activity assessment*

The in vitro assessment of antioxidant activity was conducted using the DPPH (2,2-diphenyl-1-picrylhydrazyl) radical scavenging assay. In this protocol, 400 µl of methanolic solutions of the test compounds,

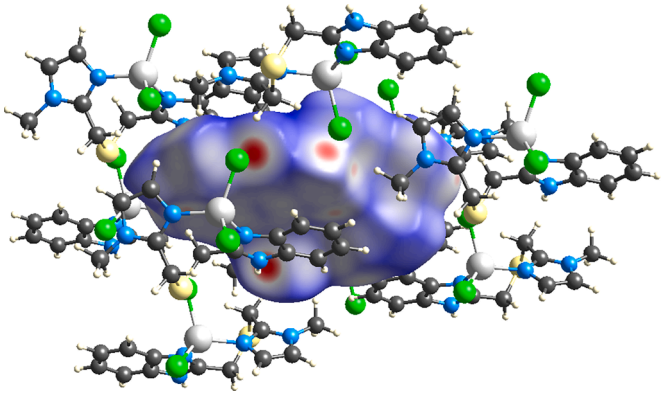

Fig. 7. Positions of the intermolecular interactions due to the molecular environment around complex Zn(MIMTMB)Cl_2.

MIMTMB and its zinc complex, Zn(MIMTMB)Cl_2, at a concentration of 4 mM were added to 800 μl of a 0.19 mM DPPH solution prepared in methanol (MeOH). The reaction mixtures were thoroughly mixed and incubated in the dark at room temperature for 30 min. This incubation period allowed for the reaction between the antioxidant compounds and the DPPH radicals, during which the reduction of the DPPH radicals by hydrogen atoms donated by the antioxidant compounds resulted in a color change from purple to yellow or colorless.

Following the incubation period, the absorbance of the reaction mixtures was measured spectrophotometrically at 517 nm. The decrease in absorbance indicated the scavenging activity of the test compounds against the DPPH radicals, with greater reductions in absorbance corresponding to higher antioxidant activity. The percentage inhibition of DPPH radicals by each compound was calculated using the formula:

$$\text{Inhibition \%} = \frac{\text{Absorbance of control} - \text{Absorbance of sample}}{\text{Absorbance of control}} \times 100$$

All experiments were conducted in quadruplicate to ensure reproducibility and statistical analysis was performed to determine significant differences between the test compounds and the control, following standardized protocols.

2.4. Molecular docking

Molecular docking investigation of the antioxidant activity was conducted using the AutoDock Vina algorithm within Chimera 1.15. First, the three-dimensional structure of the cytochrome c peroxidase (CCP) enzyme (PDB code: 2 × 08) was retrieved from the Protein Data Bank. The ligands, including the reference molecule ascorbate and the designed compounds MIMTMB and its zinc complex, Zn(MIMTMB)Cl_2, were prepared using Chimera tools to optimize their structures and generate appropriate ligand files for docking. The receptor grid was defined around the active site of CCP, ensuring that key residues involved in ligand binding were included. Docking calculations were performed using AutoDock Vina, employing a grid-based docking approach to predict the binding conformations and affinities of the ligands within the active site of CCP. The docking protocol was validated through re-docking of the co-crystallized ligand, ascorbate, and assessing the root-mean-square deviation (RMSD) between the predicted and crystallographic poses. The resulting docking poses were then analyzed and visualized using Discovery Studio and PyMOL software, allowing for the examination of 2D and 3D interactions between the ligands and CCP.

2.5. Drug-likeness and ADMET properties

The drug-likeness of the compound MIMTMB was evaluated using the SwissADME online tool (http://www.swissadme.ch/), which assesses various physicochemical properties relevant to the pharmacokinetics and bioavailability of potential drug candidates. The chemical structure of MIMTMB was prepared in SMILES format and input into the SwissADME tool, which then calculated key physicochemical parameters such as molecular weight (MW), logarithm of the octanol-water partition coefficient (LogP), number of hydrogen bond donors (HBD), number of hydrogen bond acceptors (HBA), topological polar surface area (TPSA), and the number of rotatable bonds (nRB). These parameters were analyzed against Lipinski's Rule of Five, which includes criteria for MW (<500 g/mol), LogP (<5), HBD (no >5), and HBA (no >10). Additionally, the compound was evaluated against the Veber Rule, which considers TPSA (<140 Å^2) and nRB (<10), to further predict its oral bioavailability.

For the ADMET (Absorption, Distribution, Metabolism, Excretion, and Toxicity) analysis, the ADMET properties of MIMTMB were investigated using the admetSAR tool. The compound's SMILES format was input into admetSAR (http://lmmd.ecust.edu.cn/admetsar2), which provided a comprehensive profile including blood-brain barrier (BBB) penetration, Caco-2 cell permeability, human intestinal absorption, human oral bioavailability, P-glycoprotein inhibition, and inhibition of cytochrome P450 enzymes (CYPs). Furthermore, the tool assessed potential toxicological properties such as hepatotoxicity, respiratory toxicity, carcinogenicity, and skin and eye corrosion.

3. Results and discussion

3.1. Chemistry

The ligand MIMTMB was obtained by the action of (1H-benzo[d] imidazol-2-yl)methanethiol on 2-chloromethyl-1-methyl-1H-imidazole in anhydrous MeOH and in the presence of sodium methoxide. The structure of the ligand MIMTMB obtained was confirmed by spectroscopic methods (IR, ^{1}H NMR and X-ray). Examination of the ^{1}H NMR spectrum of MIMTMB shows the appearance of a singlet at approximately 3.75 ppm, corresponding to the methylene group linked to benzimidazole ring. The methylene and methyl group linked to the imidazole ring appeared at 3.79 ppm. The aromatic protons appeared between 7.68 and 6.97 ppm. The broad singlet at approximately 12.38 ppm corresponds to the NH proton of benzimidazole ring. In the ^{13}C NMR spectrum, a signal at 33.22 ppm is observed, characteristic of the methyl group. Two signals at approximately 26.98 ppm and 25.36 ppm, characteristic of the two CH_2 groups. The aromatic carbons resonate between 115.4 and 151.62 ppm.

The corresponding complex Zn(MIMTMB)Cl_2 was obtained from reaction of an equimolar amount of $ZnCl_2$ and ligand MIMTMB in methanol with a 71 % yield. The complex was characterized by spectroscopic methods and elemental analysis. The ^{1}H NMR spectrum of Zn(MIMTMB)Cl_2 shows that aromatic protons appeared between 8.57 and 7.46 ppm and the signal of the NH proton of benzimidazole ring appeared at approximately 13.85 ppm. The methyl group linked to the imidazole ring appeared at 4.10 ppm. The ^{13}C NMR spectrum shows that aromatic carbons resonate between 152.79 and 112.59 ppm. The carbone of the methyl group linked to the imidazole ring appeared at 33.35 ppm.

The ligand and its Zinc complex are stable at room temperature, non-hygroscopic, and partially soluble in methanol and ethanol. The reactions are shown in the following scheme 1.

3.2. Crystallographic study

Suitable crystals for X-ray diffraction were obtained by slow evaporation at room temperature from concentrated MeOH solution of MIMTMB. For complex Zn(MIMTMB)Cl_2, suitable crystals for X-ray diffraction were collected by slow evaporation at room temperature of the corresponding DMF solution and both structures were confirmed by X-ray crystal structure analysis. The refined crystalline structure of X-ray is represented in Fig. 1 and the crystallographic data, recording

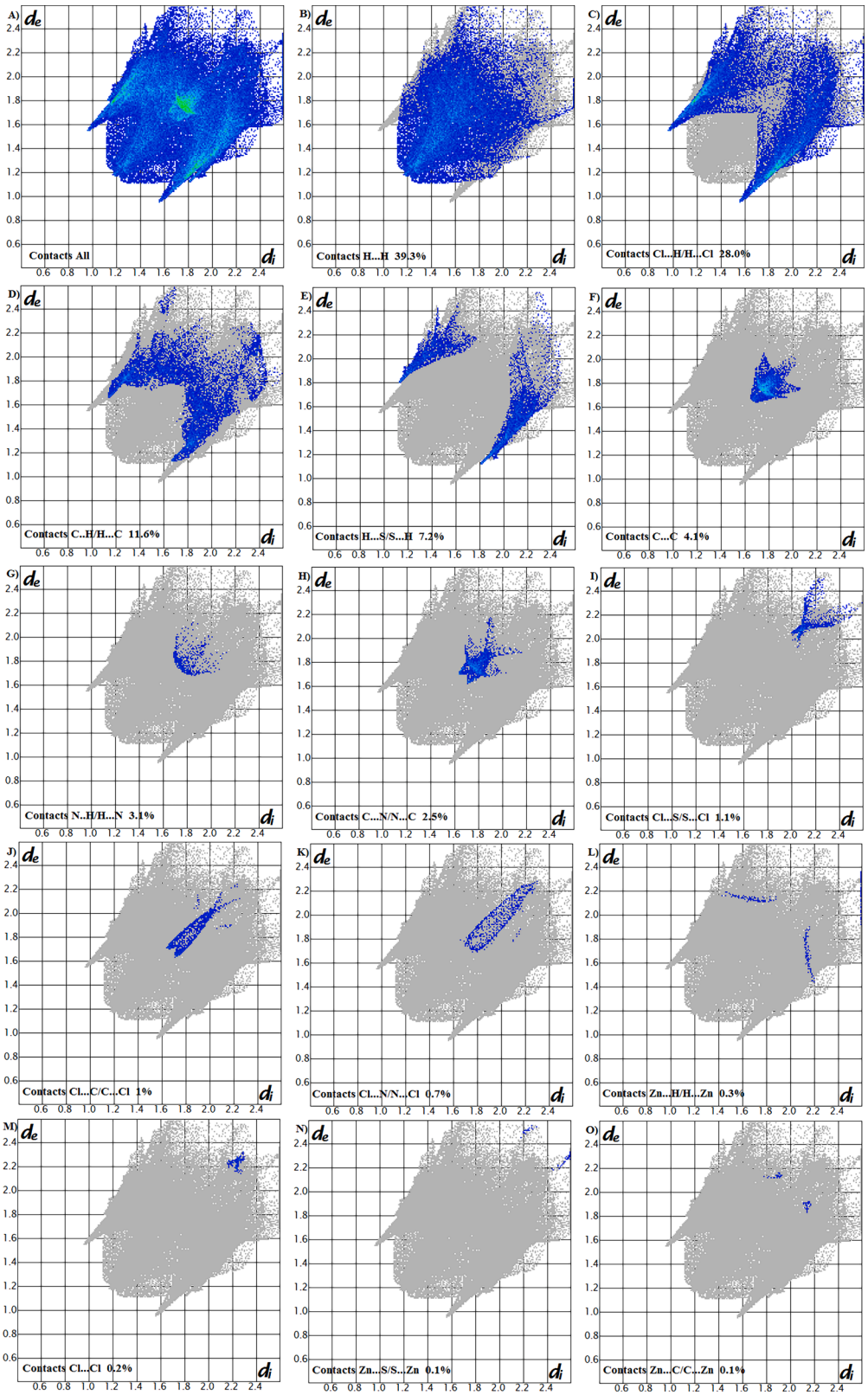

Fig. 8. 2D graphs showing the contribution of intermolecular interactions to the Hirshfeld surface surrounding complex Zn(MIMTMB)Cl_2.

conditions, and refinement results are summarized in Table 1.

3.2.1. *Crystal structure, packing and molecular interactions of MIMTMB*

The ligand 2-(1-methyl-1H-imidazol-2-ylmethylthio)methyl-1H-benzimidazole (MIMTMB) crystallizes in the non-centrosymmetric Orthorhombic crystal system (space group $P\ 2_12_12_1$). The asymmetric unit contains two co-crystallized water molecules and one ligand molecule. This organic molecule consists of a benzimidazole unit connected to an imidazole fragment by two methylene groups and a sulfur atom. The two molecules, benzimidazole and imidazole, form a dihedral

Table 5
Antioxidant activity of the ligand MIMTMB and its complex.

Molecules	DPPH inhibition percentage
MIMTMB	44.80±2,44[§]
$Zn(MIMTMB)Cl_2$	14.84±1,60[#]

The values represent the mean ± standard deviation established in quadruplicate ($n = 4$). Statistics: the same symbols *, §, $, ‡, or # indicate that the values are significantly different ($P < 0.05$) from others as determined by one-way ANOVA followed by Newman-Keuls multiple comparison test.

Table 6
Docking results of the reference molecule ascorbate, MIMTMB, and Zn $(MIMTMB)Cl_2$ complex within the binding pocket of cytochrome c peroxidase (PDB ID: 2 × 08).

Compound	Binding energy (Kcal/mol)	Hydrogen interactions (Distance Å)	Hydrophobic interactions	Electrostatic interactions
Ascorbate (Co-crystallized ligand)	−6.2	Arg184 (2.65), Val45 (2.81), Tyr42 (3.71), His181 (2.87)	–	–
MIMTMB	−5.7	Arg184 (3.13), Gly41(2.62), Asp37 (3.37)	His181, Val45, Tyr42, Ala36, Pro44	Asp37
Zn(MIMTMB) Cl_2 complex	−2.4	–	Ile40, Ala36, Pro44, Arg48, Val45	Arg184, Asp37

angle of 58.54° The C—N bond lengths, C(1)–N(1) (1.402(2)Å), C(6)–N (3) (1.384(2)Å), C(7)–N(1) (1.324(2)Å), C(7)–N(3) (1.350(2)Å), C(8)–N (2) (1.320(3)Å), C(8)–N(4) (1.354(3)Å), C(9)–N(2) (1.376(3) Å), C(10)–N(4) (1.361(3)Å), C(11)– N(4) (1.447(3) Å), are close to each other and reported in Table 2. The (MIMTMB) ligand display very normal bond angles. The bond angles N(1)–C(7)–N(3) and N(2)–C(8)–N(4) are 113.04 (17)° and 111.37(19)°, respectively, and the bond angle N(1)–C(7)–C (13) is 124.12(18)°. Other values of the lengths and angles between the atoms of the (MIMTMB) ligand are grouped in Table 2.

The crystal as a whole can be described as an alternation of zigzag double layers along the c-axis parallel to the (100) plane (Fig. 2a). These layers are interconnected with hydrogen bonding interactions O-H...N, C-H...O, N-H...O, and O-H...O, resulting in the formation of three-dimensional networks. The hydrogen bond between the water molecule forms a chain with a set of graph motifs ($D_1^1(2)$, where the water molecule serves two roles as an acceptor and donor (Fig. 2b).Other hydrogen bonding parameters are listed in Table 3.

The whole structure is consolidated by π−π stacking interactions with a centroid-to-centroid distance of 3.624(4) Å. Additionally, there is a weak intermolecular interaction C(13)-H(13A)…Cg (N(1)-C(1)-C(6)-N (3)-C(7)) with a C…Cg distance of 3.539(5) Å and a C—H…Cg angle of 123° These interactions connect molecules between layers and also link the layers together, enhancing the cohesion of the organic structure (Table 4 and Fig. 2c).

3.2.2. Crystal structure, packing and molecular interactions of complex Zn (MIMTMB)Cl_2

X-ray diffraction revealed that the asymmetric unit contains a single molecule of the complex $Zn(MIMTMB)Cl_2$, which is depicted in Fig. 1. The complex $Zn(MIMTMB)Cl_2$ with the formula $C_{13}H_{14}C_{l2}ZnN_4S$ crystallizes in space group $P2_1/c$ of the monoclinic system, with the following linear and angular parameters: $a = 7.6464(3)$ Å, $b = 16.0038$ (6) Å, $c = 13.5503(5)$ Å, $\beta = 111.114(2)°$, with $Z = 4$.

The complex $Zn(MIMTMB)Cl_2$ exhibit a distorted tetrahedral geometry with a zinc atom at the center of the tetrahedron. The Zinc atom is surrounded by two chlorine atoms in *cis* position and by two nitrogen atoms (N1 and N2) from the ligand (MIMTMB). The two ligand moieties, benzimidazole and imidazole, are not coplanar structure, subtending a dihedral angle of 60.12 (2). The bond distances Zn1–N1 and Zn1– N2 are 2.0416(11) and 2.0173(12) Å, respectively, while the distance Zn1–Cl1 is 2.2561(5) Å and the distance Zn1–Cl2 is 2.2375(4) Å. Bond angles N1–Zn1–Cl1 and Cl1–Zn1–Cl2 are 107.39(4)° and 113.182(18)°, respectively and the bond angle N1–Zn1–N2 is 106.79(5) Å. The deviation of these values from the ideal value of 109° corresponding to the perfect tetrahedral geometry indicates some distortion. The bond distances and angle values are in the normal ranges and are comparable to the corresponding bonds found in similar complexes [24].

The crystal stacking for this complex is in the form of layers, arranged parallel to the crystallographic plane (101). The crystal packing and cohesion are ensured by the presence of intermolecular hydrogen bond interactions of the N-H…Cl and C-H…Cl types, which form chains and cycles with graphs sets motif $R_2^2(12)$ and $C_1^1(6)$, respectively, as well as intramolecular hydrogen bonds of the C-H…N type, whose characteristics are summarized in Table 3 and represented in Fig. 3b. In this complex, crystal cohesion is also ensured by π-π (3.622 (3) Å) and C-H...π interactions (Table 4 and Fig. 3c).

3.3. Hirshfeld surfaces analysis

Since it sheds more light on the weak intermolecular interactions in the crystal structure, the study of calculated Hirshfeld surfaces is very beneficial [25]. To locate any atom-atom short contacts that can form hydrogen bonds and figure out the quantitative ratios of these interactions, in addition to any π-stacking interactions [26,27].

Analysis of the Hirshfeld surface of the MIMTMB ligand allowed us to determine the contacts between the atoms of this molecule and those of the rest of the crystal. Examination of the dnorm representation mode of the Hirshfeld surface (Fig. 4) reveals the presence of red spots distributed in a heterogeneous manner and allows us to identify the shortest contacts present in the structure

The examination of the 2D fingerprint plots reveals the contribution of intermolecular interactions depicted on the Hirshfeld surfaces. Fig. 5 illustrates the 2D plot of all the contacts contributing to the Hirshfeld surface encompassing the MIMTMB ligand.

Fig. 6 illustrates the percentage contribution of different types of contacts to the total Hirshfeld surface. It is worth noting that the majority of intermolecular interactions are of the H…H type with a contribution of 54.2 %. As for C…H/H…C contacts, they contribute 16.3 %, followed by O…H/H…O contacts (10.3 %), S…H/H…S (7.8 %), N…H/H…N (6.6 %), and C..C (2.8 %). The remaining contacts represent only 1.9 % of the Hirshfeld surface, with 1.6 % of C…N/N…C and 0.3 % of S…S.

The intermolecular interactions, resulting from the molecular environment of the complex $Zn(MIMTMB)Cl_2$ presented with red spots (Fig. 7), were determined by establishing the Hirshfeld surface around it

The Fig. 8 illustrates the 2D plot derived from all contacts contributing to the Hirshfeld surface around the crystal $Zn(MIMTMB)Cl_2$. H…H contacts represent a contribution of (39.3 %) to the Hirshfeld surface around the compound. These contacts are followed by Cl…H/H…Cl contacts (28.0 %), C…H/H…C (11.6 %), H…S/S…H (7.2 %), C…C (4.1 %), N…H/H…N (3.1 %), C…N/N…C (2.5 %), Cl…S/S…Cl (1.1 %), and Cl…C/C…Cl (1 %). As for the weaker contacts like Cl…N/N…Cl, Zn…H/H…Zn, Cl…Cl, Zn…S/S…Zn, and Zn…C/C…Zn, each of them contributes <1.0 % to the total observed intermolecular interactions.

3.4. In vitro antioxidant activity assessment

The antioxidant activities of MIMTMB and its zinc complex Zn $(MIMTMB)Cl_2$ were evaluated using the DPPH radical scavenging assay. The results indicated a significant difference between the two

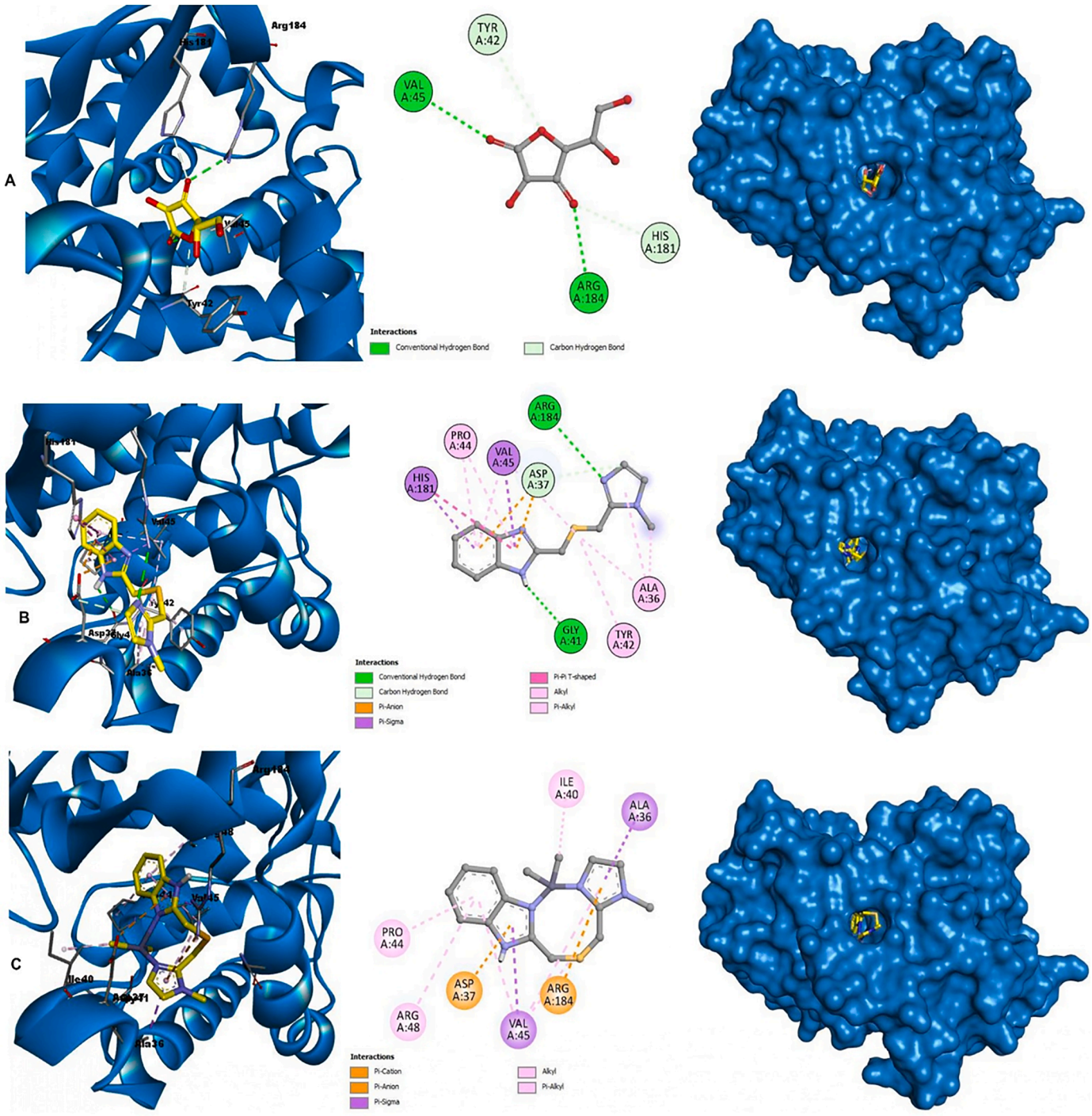

Fig. 9. Docking-generated 2D and 3D representations of the reference molecule ascorbate (A), MIMTMB (B), and Zn(MIMTMB)Cl_2 complex (C) within the binding pocket of cytochrome c peroxidase (PDB ID: 2 × 08).

Table 7
Drug-likeness properties of MIMTMB.

	MW g/mol	Log S	LogP	HBD	HBA	nRB	TPSA (Å^2)	AMR	Lipinski	Ghose	Veber	Egan
MIMTMB	258.34	−4.43	0.09	1	4	4	40.57	80.47	Yes	No	Yes	Yes

compounds (Table 5). MIMTMB demonstrated a notable inhibition of DPPH radicals, achieving a percentage inhibition of 44.80 % ± 2.44. Conversely, the Zn(MIMTMB)Cl_2 complex exhibited a considerably lower antioxidant activity, with a percentage inhibition of 14.84 % ± 1.60.

These results highlight the superior antioxidant activity of MIMTMB compared to its zinc complex. The higher percentage of DPPH inhibition by MIMTMB suggests that it has a stronger ability to neutralize free radicals. The substantial difference in activity between MIMTMB and Zn(MIMTMB)Cl_2 may be attributed to differences in their chemical

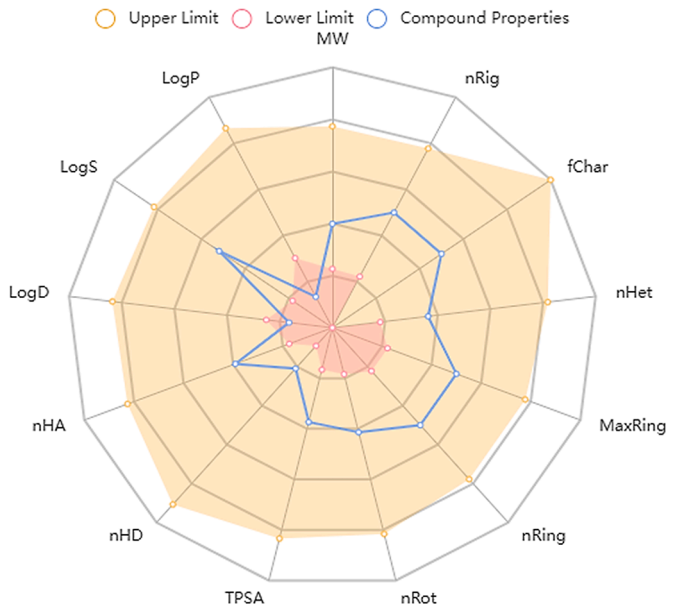

Fig. 10. Physicochemical space for the MIMTMB presented in bioavailability radar analysis. The pink area defines the lower limit and the orange area defines the upper limit for each property which are Molecular Weight (MW), Number of hydrogen bond acceptors (*nHA),* Number of hydrogen bond donors (*nHD),* number of rotatable bonds (*nRot*), number of rings. *(nRing),* number of atoms in the biggest ring. *MaxRing,* Number of heteroatoms. *nHet* Formal charge. (*fChar),* Number of rigid bonds *(nRig),* Topological polar surface area. (*TPSA)* aqueous solubility log*S* n-octanol/water distribution coefficient log*P* n-octanol/water distribution coefficients at pH=7.4 log*D7.4*.

Table 8
ADMET properties of MIMTMB.

	Criteria	Value	Probability
Absorption-Distribution	BBB penetration	+	0.9250
	Caco2	+	0.5000
	Human Intestinal Absorption	+	0.9935
	Human oral bioavailability	+	0.6571
Metabolism	P-glycoprotein inhibitor	–	0.9184
	CYP2C19 inhibitor	–	0.7724
	CYP3A4 inhibitor	–	0.9269
	CYP2C8 inhibitor	–	0.7203
	CYP2D6 inhibitor	–	0.7579
	CYP2C9 inhibitor	–	0.8931
	CYP1A2 inhibitor	–	0.6378
Excretion	Clearance	Moderate	
Toxicity	Human Ether-a-go-go-Related Gene inhibition	–	0.6569
	Carcinogenicity	–	0.9300
	Eye Corrosion	–	0.9353
	Skin corrosion	–	0.6411
	Ames mutagenesis	–	0.6000
	Hepatotoxicity	+	0.6250
	Respiratory toxicity	+	0.6889
	Estrogen receptor binding	+	0.6041
	Androgen receptor binding	+	0.5251
	Nephrotoxicity	–	0.6657
	Thyroid receptor binding	–	0.4878
	Glucocorticoid receptor binding	–	0.4677

structures and the potential influence of zinc on the antioxidant properties of the complex.

The reduced activity of the Zn(MIMTMB)Cl_2 complex could be due to several factors, including possible conformational changes upon complexation with zinc, which might affect the availability or reactivity of functional groups critical for antioxidant activity. Additionally, the presence of zinc might alter the solubility or stability of the complex in the assay conditions, thereby influencing its ability to interact with and neutralize DPPH radicals effectively.

The results suggest that MIMTMB alone is a more potent antioxidant than its zinc complex form. This information is crucial for understanding the structure-activity relationship and can guide the design of more effective antioxidant compounds in the future.

3.5. Molecular docking

The docking protocol underwent validation through re-docking of the co-crystallized ligand, ascorbate, within the active site of cytochrome c peroxidase. The re-docking process yielded a root-mean-square deviation (RMSD) value of 0.981 Å, indicative of the accuracy of the docking procedure. Moreover, the binding score obtained for the ascorbate (−6.2 Kcal/mol) was consistent with previous studies [28,29], reaffirming the reliability of the docking setup. Notably, all essential interactions between the co-crystallized ligand, ascorbate, and key amino acid residues within the binding site were successfully reproduced, further validating the docking methodology employed.

The docking results presented in Table 6 and Fig. 9 shed light on the potential antioxidant activities of MIMTMB and its zinc complex, Zn(MIMTMB)Cl_2, within the binding pocket of cytochrome c peroxidase (PDB ID: 2 × 08), in comparison with the co-crystallized ligand, ascorbate. These findings are particularly intriguing when correlated with the in vitro antioxidant activity results obtained through the DPPH assay.

The docking results indicate that MIMTMB exhibits a good binding energy of −5.7 Kcal/mol compared to ascorbate −6.2 Kcal/mol, suggesting a strong interaction within the binding pocket of cytochrome c peroxidase. This enhanced binding affinity of MIMTMB may be indicative of its high reactivity with CCP, contributing to its observed higher antioxidant activity in vitro.

The enhanced binding affinity of MIMTMB may contribute to its higher antioxidant activity observed in vitro, as evidenced by the significant inhibition of DPPH radicals (44.80 % ± 2.44) compared to the zinc complex, Zn(MIMTMB)Cl_2 (14.84 % ± 1.60). Moreover, the specific interactions identified through molecular docking provide further insights into the mechanisms underlying the observed antioxidant activities. MIMTMB forms hydrogen bonds with key residues such as Arg184, Gly41, and Asp37, while also engaging in hydrophobic interactions with His181, Val45, Tyr42, Ala36, and Pro44. Additionally, electrostatic interactions with Asp37 further stabilize the MIMTMB binding within the active site of cytochrome c peroxidase.

In addition to these findings, the hypothetical mode of action of these compounds warrants exploration. It's plausible that MIMTMB, with its strong binding affinity and specific interactions, may facilitate a close association with the active site of cytochrome c peroxidase, thereby modulating its catalytic activity and potentially reducing the generation of reactive oxygen species (ROS).

In contrast, the zinc complex, Zn(MIMTMB)Cl_2, exhibits a weaker binding energy (−2.4 Kcal/mol) and fewer interactions within the binding pocket compared to both MIMTMB and ascorbate. This reduction in binding affinity may account for its comparatively lower antioxidant activity observed in vitro. The interaction profile of the complex primarily shows interactions with Ile40, Ala36, Pro44, Arg48, and Val45, but lacks hydrogen bonds and notably misses interactions with key residues associated with antioxidant activity. In this case, the presence of zinc in the Zn(MIMTMB)Cl_2 complex may confer additional properties that influence its interaction with the enzyme. The weaker binding affinity of the complex suggests a possible role for zinc in modulating the conformational dynamics of the binding pocket, thereby affecting the enzyme's stability.

3.6. Drug-likeness and ADMET properties

The drug-likeness properties of MIMTMB, as summarized in Table 7 and Fig. 10, indicate promising characteristics for its potential as a

therapeutic agent. With a molecular weight of 258.34 g/mol and a LogP value of 0.09, MIMTMB demonstrates favorable properties according to Lipinski's Rule of Five, suggesting its potential suitability as a drug candidate. The presence of one hydrogen bond donor (HBD) and four hydrogen bond acceptors (HBA) aligns with typical pharmacophore profiles of bioactive compounds. Notably, MIMTMB adheres to Lipinski's Rule of Five and the Veber Rule, indicating its potential for oral bioavailability and favorable pharmacokinetic properties.

The evaluation of MIMTMB's ADMET properties, as delineated in Table 7, provides critical insights into its pharmacokinetic behavior and potential safety concerns. MIMTMB demonstrates favorable attributes across various aspects of absorption, distribution, metabolism, and excretion (ADME), revealing its potential therapeutic applicability. Notably, MIMTMB exhibits promising blood-brain barrier (BBB) penetration, suggesting its ability to access the central nervous system and potentially exert pharmacological effects in neurological disorders. Furthermore, MIMTMB demonstrates high probabilities of human intestinal absorption and oral bioavailability, indicating its suitability for systemic administration via the oral route, which is advantageous for clinical use.

Despite these promising characteristics, certain caveats warrant consideration regarding MIMTMB's pharmacological profile. Although MIMTMB does not exhibit inhibitory effects on major cytochrome P450 enzymes (CYPs), it does not display inhibition of P-glycoprotein, an ATP-dependent drug efflux transporter responsible for modulating the bioavailability and distribution of various compounds. Moreover, the ADMET assessment reveals potential concerns regarding hepatotoxicity and respiratory toxicity associated with MIMTMB. Table 8

4. Conclusion

In conclusion, we have synthesized the ligand 2-(((1-methyl-1H-imidazol-2 yl)methyl)sulfanyl)methyl)−1H-benzo[d]imidazole (MIMTMB) and its Zn(II) complex namely Zn(MIMTMB)Cl_2. Spectroscopic methods characterized both complexes and their structures were confirmed by X-ray crystal structure analysis. The single crystal X-ray analyses reveal that the centrosymmetric Zn(II) cation Zn(MIMTMB)$_2Cl_2$ complex is tetrahedrally coordinated by two N chelating azole ligand and by two chlorine atoms in a distorted tetrahedral geometry. Hydrogen-bonding interactions help to consolidate both crystal structures. In ligand MIMTMB, the layers are connected with N–H···O, C–H···O and O–H···N interactions resulting in the formation of two-dimensional networks. In Zn(MIMTMB)$_2Cl_2$ complex, the cohesion of the structure and stability are ensured by intermolecular N–H···Cl, Cl–H··· Cl and C–H···N hydrogen bonds. The intermolecular interactions in complex and ligand are further inspected by Hirshfeld surface analysis. This study highlights also the promising antioxidant activity of MIMTMB, supported by its strong binding affinity to cytochrome c peroxidase (CCP) and significant inhibition of DPPH radicals in vitro. Conversely, the zinc complex, Zn(MIMTMB)Cl_2, exhibits weaker antioxidant activity, possibly due to alterations in its interaction profile induced by zinc. Moreover, the assessment of MIMTMB's ADMET and drug-likeness properties revealed its potential as a therapeutic agent, demonstrating high probabilities of human intestinal absorption and oral bioavailability. These findings suggest its suitability for systemic administration, opening avenues for further exploration and development as a pharmaceutical candidate.

CRediT authorship contribution statement

Feriel Aouatef Sahki: Investigation. **Mehdi Bouchouit:** Writing – original draft. **Ouided Benslama:** Writing – original draft, Software, Investigation. **Rafika Bouchene:** Investigation. **Sofiane Bouacida:** Investigation. **Abdelmalek Bouraiou:** Writing – review & editing, Writing – original draft, Methodology, Investigation.

Declaration of competing interest

The authors declare that they have no known competing financial interests or personal relationships that could have appeared to influence the work reported in this paper.

Supplementary materials

Supplementary material associated with this article can be found, in the online version, at doi:10.1016/j.molstruc.2024.141034.

Data availability

No data was used for the research described in the article.

References

[1] B. Biswas, S. Salunke-Gawali, T. Weyhermuller, V. Bachler, E. Bill, P. Chaudhuri, Metal-complexes as ligands to generate asymmetric homo- and heterodinuclear MAIIIMBII species: a magneto-structural and spectroscopic comparison of imidazole-N versus pyridine-N, Inorg. Chem. 49 (2010) 626–641, https://doi.org/10.1021/ic9018426.
[2] S.S. Chen, The roles of imidazole ligands in coordination supramolecular systems, CrystEngComm 18 (2016) 6543–6565, https://doi.org/10.1039/c6ce01258b.
[3] P.J. Steel, Aromatic nitrogen heterocycles as bridging ligands; a survey, Coord. Chem. Rev. 106 (1990) 227–265, https://doi.org/10.1016/0010-8545(60)80005, 7.
[4] M. Andersson Trojer, A. Movahedi, H. Blanck, M. Nydén, Imidazole and triazole coordination chemistry for antifouling coatings, J. Chem. (2013) 946739, https://doi.org/10.1155/2013/946739, 2013.
[5] M.R. Malachowski, M.E. Adams, D. Murray, R. White, N. Elia, A.L. Rheingold, L. N. Zakharov, R.S. Kelly, Copper(II) complexes of bidentate ligands containing nitrogen and sulfur donors: synthesis, structures, electrochemistry and catalytic properties, Inorganica Chim. Acta 362 (4) (2009) 1247–1252, https://doi.org/10.1016/j.ica.2008.06.008.
[6] R.D. Hancock, L.J. Bartolotti, A DFT study of the affinity of lanthanide and actinide ions for sulfur-donor and nitrogen-donor ligands in aqueous solution, Inorg. Chim. Acta 396 (2013) 101–107, https://doi.org/10.1016/j.ica.2012.10.010.
[7] Ş. Karadeniz, C.Y. Ataol, O. Şahin, Ö. İdil, Hü. Bati, Synthesis, structural studies and antimicrobial activity of N'-((2Z, 3E)-3- (hydroxyimino)butan-2-ylidene)-2-phenylacetohydrazide and its Co(II), Ni(II) complexes, J. Mol. Struct. 1161 (2018) 477–485, https://doi.org/10.1016/j.molstruc.2018.01.087.
[8] R.Ahmad Shiekh, I. Ab Rahman, M.A. Malik, N. Luddin, S.M. Masudi, S.A. Al-Thabaiti, Transition metal complexes with mixed nitrogen-sulphur (N-S) donor macrocyclic schiff base ligand: synthesis, spectral, electrochemical and antimicrobial studies, Int. J. Electrochem. Sci. 8 (2013) 6972–6987, https://doi.org/10.1016/S1452-3981(23)14821-8.
[9] G. Steel, A. Mustapha, J. Reglinski, A.R. Kennedy, The nickel, copper and zinc complexes of potentially heptadentate nitrogen–sulfur donor ligands, Polyhedron 67 (2014) 360–367, https://doi.org/10.1016/j.poly.2013.09.018.
[10] R.V. Singh, Pratibha Chaudhary, Kavita Poonia, Shikha Chauhan, Microwave-assisted synthesis, characterization and biological screening of nitrogen–sulphur and nitrogen–oxygen donor ligands and their organotin(IV) complexes, Spectrochim. Acta Part A Mol. Biomol. Spectrosc. 70 (3) (2008) 587–594, https://doi.org/10.1016/j.saa.2007.08.002.
[11] A.K. Sharma, S. Chandra, Complexation of nitrogen and sulphur donor Schiff's base ligand to Cr(III) and Ni(II) metal ions: synthesis, spectroscopic and antipathogenic studies, Spectrochim. Acta A Mol. Biomol. Spectrosc. 78 (1) (2011) 337–342, https://doi.org/10.1016/j.saa.2010.10.017.
[12] B. Soltani, M. Ghorbanpour, C.J. Ziegler, M. Ebadi-Nahari, R. Mohammad-Rezaei, a Nickel, II) and cobalt (II) complexes with bidentate nitrogen-sulfur donor pyrazole derivative ligands: syntheses, characterization, X-ray structure, electrochemical studies, and antibacterial activity, Polyhedron 180 (2020) 114423, https://doi.org/10.1016/j.poly.2020.114423.
[13] A.B. Jena, R.R. Samal, N.K. Bhol, A.K. Duttaroy, Cellular Red-Ox system in health and disease, Biomed. Pharmacother. 162 (2023) 114606, https://doi.org/10.1016/j.biopha.2023.114606.
[14] D. Martins, M. Kathiresan, A.M. English, Cytochrome c peroxidase is a mitochondrial heme-based H_2O_2 sensor that modulates antioxidant defense, Free Radic. Biol. Med. 65 (2013) 541–551, https://doi.org/10.1016/j.freeradbiomed.2013.06.037.
[15] V.B. Borisov, S.A. Siletsky, M.R. Nastasi, E. Forte, ROS defense systems and terminal oxidases in bacteria, Antioxidants 10 (6) (2021) 839, https://doi.org/10.3390/antiox10060839.
[16] A. Benhassine, H. Boulebd, B. Anak, M.Kara Ali, A. Bouraiou, H. Merazig, N. Kacem-Chaouche, A. Belfaitah, Co(II) complexes derived from (1-methyl-1H-imidazol-2-yl)methanol: synthesis, characterization, spectroscopic study, DFT/TD-DFT calculations and biological evaluation, Inorg. Chim. Acta 497 (2019) 119073, https://doi.org/10.1016/j.ica.2019.119073.
[17] M. Bouchouit, S. Bouacida, B. Zouchoune, H. Merazig, S. Bua, Z. Bouaziz, M. Le Borgne, C.T. Supuran, A. Bouraiou, Synthesis, X-ray structure, in silico calculation,

and carbonic anhydrase inhibitory properties of benzylimidazole metal complexes, J. Enzyme Inhib. Med. Chem. 33 (2018) 1150–1159, https://doi.org/10.1080/14756366.2018.1481404.
[18] M. Bouchouit, H. Belahlou, M. Guergouri, R. Bensegueni, S. Bouacida, E. Bendeife, K. Bouchouit, A. Bouraiou, Synthesis, characterization and structural study of new nickel(II) and mercury (II) complexes with imidazole oxime ligand, J. Mol. Struct. 1287 (2023) 135674, https://doi.org/10.1016/j.molstruc.2023.135674.
[19] R. Kerkatou, H. Belahlou, M. Bouchouit, F. Berrah, S. Bouacida, K. Bouchouit, A. Bouraiou, Synthesis, characterization and structural study of two imidazole oxime ligand and their ZnII mononuclear coordination compounds, J. Mol. Struct. 1294 (2023) 136545, https://doi.org/10.1016/j.molstruc.2023.136545.
[20] M.C. Burla, R. Caliandro, M. Camalli, B. Carrozzini, G.L. Cascarano, L. De Caro, C. Giacovazzo, G. Polidori, R. Spagna, SIR2004: an improved tool for crystal structure determination and refinement, J. Appl. Cryst. 38 (2005) 381–388, https://doi.org/10.1107/S002188980403225X.
[21] G.M. Sheldrick, A short history of SHELX, Acta Cryst. A 64 (2008) 112–122, https://doi.org/10.1107/S0108767307043930.
[22] L.J. Farrugia, WinGX and ORTEP for windows: an update, J. Appl. Cryst. 45 (2012) 849–854, https://doi.org/10.1107/S0021889812029111.
[23] G.M. Sheldrick, SADABS, Bruker AXS Inc, Madison, Wisconsin, USA, 2002.
[24] M. Bouchouit, M.E. Said, M.Kara Ali, S. Bouacida, H. Merazig, N. Kacem Chaouche, A. Chibani, B. Zouchoune, A. Belfaitah, A. Bouraiou, Synthesis, X-ray structure, theoretical investigation, corrosion inhibition and antimicrobial activity of benzimidazole thioether and theirs metal complexes, Polyhedron 119 (2016) 248–259, https://doi.org/10.1016/j.poly.2016.08.045.
[25] M.A. Spackman, J.J. McKinnon, Fingerprinting intermolecular interactions in molecular crystals, CrystEngComm 4 (2002) 378–381, https://doi.org/10.1039/B203191B.
[26] J.J. McKinnon, A.S. Mitchell, M.A. Spackman, Hirshfeld surfaces: a new tool for visualising and exploring molecular crystals, Chem. Eur. J. 4 (1998) 2136–2140, https://doi.org/10.1002/(SICI)1521-3765(19981102)4, 11<2136::AID−CHEM2136>3.0.CO;2-G.
[27] J.J. McKinnon, M.A. Spackman, A.S. Mitchell, Novel tools for visualizing and exploring intermolecular interactions in molecular crystals, Acta Crystallogr. Sect. B 60 (60) (2004) 627–632, https://doi.org/10.1107/S0108768104020300.
[28] M.S. Abdelrahim, A.M. Abdel-Baky, S.A. Bayoumi, E.Y. Backheet, Antioxidant and antidiabetic flavonoids from the leaves of Dypsis pembana (H.E.Moore) Beentje & J.Dransf., Arecaceae: in vitro and molecular docking studies, BMC Complement. Med. Ther. 23 (2023) 440, https://doi.org/10.1186/s12906-023-04287-z.
[29] W.S. Shehab, M.A. Aziz, N.K.R. Elhoseni, M.G. Assy, M.H. Abdellattif, E.O. Hamed, Design, synthesis, molecular docking, and evaluation antioxidant and antimicrobial activities for novel 3-phenylimidazolidin-4-one and 2-aminothiazol-4-one derivatives, Molecules 27 (2022) 767, https://doi.org/10.3390/molecules27030767.